PLASMA PHYSICS GROUP

EXPERIMENTS ON PARAMETRIC INSTABILITIES IN LASER-PLASMA INTERACTIONS*

Francis F. Chen

PPG-264 June 1976

UNIVERSITY OF CALIFORNIA
LOS ANGELES

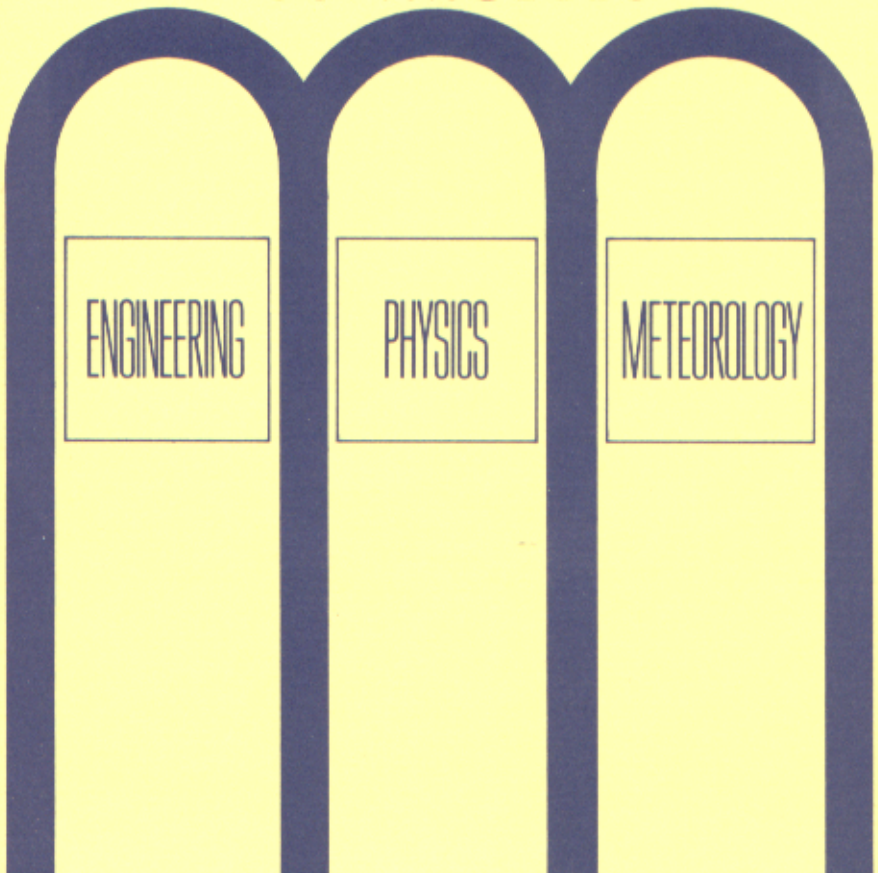

EXPERIMENTS ON PARAMETRIC INSTABILITIES IN LASER-PLASMA INTERACTIONS*

Francis F. Chen

PPG-264 June 1976

Electrical Sciences and Engineering Department
University of California
Los Angeles, California 90024

Paper presented at the Nobel Symposium on Nonlinear Effects in plasmas, Göteborg, Sweden, June 11-17, 1976

*Work supported by USERDA, Contract E(04-3)-34, P.A. 236

EXPERIMENTS ON PARAMETRIC INSTABILITIES IN LASER-PLASMA INTERACTIONS

Francis F. Chen

University of California

Los Angeles, California

Recent experiments in laser-fusion laboratories have indicated the importance of non-classical processes in the absorption of intense laser radiation by solid targets. For instance, back-scattered light typically ranges from 10% to 50% of the incident intensity, larger than can be explained by classical reflection at the critical layer; and the excess has often been attributed to a parametric instability such as stimulated Brillouin or Raman scattering. Absorption of light--typically 40%--is lower than classical inverse bremsstrahlung in some experiments and higher in others. The parametric decay and OTS (oscillating two-stream) instabilities are supposed to occur near the critical layer to enhance the absorption. Even when classical processes are sufficient to explain the observed absorption, anomalous effects are indicated by the appearance of suprathermal electrons, as revealed by x-ray spectra. An even more serious effect is the generation of fast ions, which have in some instances accounted for as much as 80% of the absorbed energy. Acceleration of ions by electric fields generated in nonlinear processes has been conjectured. Finally, experiments on transmission through and fast ions from plastic foils have shown that heat conductivity is anomalously low, thus raising the possibility of large, self-generated magnetic fields.

Because of the small size and short time scale of the experiments, confirmation of theoretically predicted plasma phenomena must necessarily rely on indirect measurements. It would be well-nigh impossible, for instance, to verify the absorption of light via the parametric decay instability by detecting the ion acoustic and electron plasma waves which are generated in the corona of an imploding pellet. Instead, one normally uses a computer code to

study the nonlinear development of a particular mechanism and to predict the macroscopic observables. In this example, the observables could include the net energy absorption and the non-thermal tail of the electron distribution (which, in turn, is measured indirectly from the x-ray spectrum). Needless to say, even if the measurements should agree with the computer simulations, the sequence of events would not be uniquely identified; in fact, even the existence of the initiating instability would not be proved.

Just as computer simulation has brought theory closer to experiment, experimental simulation in larger, less dense plasmas can bring the complex phenomena of laser-fusion closer to theory. A prime example of this is the work done with microwaves in large, tenuous plasmas. The experimental discovery by Kim, Stenzel, and Wong[1] of density depressions--"cavitons"--formed by self-trapped rf energy has led to computational predictions of solitons, profile modification, and ion acceleration. A second example is the verification of Brillouin backscattering in the CO_2-laser experiments reviewed below. Without proof that the linear effect really occurs in nature, computer extrapolations to nonlinear saturation and calculations of the resultant reflection coefficient would be on shaky ground indeed. Finally, we cite the recent investigation by Obenschain, Luhmann, and Greiling[2] of the effect of finite bandwidth pumps on parametric thresholds. In this case, theory preceded experiment; but by using microwaves, the authors were able to demonstrate control of parametric instabilities well before the technology was in hand to do so with lasers.

In toroidal-confinement fusion, the understanding of microinstabilities in stellarators and tokamaks was impeded by the simultaneous occurrence of many phenomena in the complex magnetic geometry. Progress was made only after plasma sources such as Q-machines and multipoles were devised so that the plasma could be controlled to exhibit one effect at a time. The development of suitable plasma sources is, similarly, needed for experimental unraveling of complex laser-fusion phenomena. When laser light forms a plasma from a solid target, many unnecessary complications make it difficult to study the physics of the laser-plasma interaction. For instance, a slight amount of prepulse can change the density gradient scale length and greatly affect instability thresholds. The uniformity of illumination is often poor at high intensities. Most solids, particularly tampered glass shells, have different atomic masses of high-Z atoms, giving rise to an unknown mixture of charge states that can interact. Spherical targets have refraction effects and contain a continuum of angles of incidence; even flat targets give rise to hemispherical plasmas. Expansion of the plasma causes Doppler shifts which obscure the intrinsic frequency shifts in scattered light; differential expansion can greatly affect thresholds. The density profile, important

in determination of thresholds, cannot be measured except in a crude way. Worst of all, the critical ($\omega_o = \omega_p$, $n = n_c$), quarter-critical ($\omega_o = 2\omega_p$, $n = n_c/4$), and underdense ($\omega_o > 2\omega_p$, $n < n_c/4$) regions are all present at once; and each has its own set of parametric instabilities. To remove this unnecessary complication, an obvious procedure is to employ lasers incident on gas or plasma targets which are everywhere underdense. Only a few such experiments have been done so far; these are reviewed in the next section. A relatively large body of literature exists for microwave simulations; a review of these would be outside the scope of this paper. For the reasons given above, we do not regard experiments on solid targets to be sufficiently controllable for detailed studies of laser-plasma interactions.

SURVEY OF RELEVANT EXPERIMENTS

Experiments on Backscattering in Underdense Plasmas

Anomalous reflection of light from plasmas can occur through the parametric decay of an incident photon (ω_o, $\underline{k}_o$) into a red-shifted photon (ω_2, $\underline{k}_2$) and either a plasmon (electron plasma wave) or a phonon (ion acoustic wave) (ω_i, $\underline{k}_i$). Thresholds for these processes, called respectively stimulated Raman scattering (SRS) and stimulated Brillouin scattering (SBS), were calculated for homogeneous plasmas by Drake et al.[3]. These thresholds are easily exceeded, but in a series of papers Rosenbluth, Liu, and others[4] pointed out that plasma inhomogeneity, finite interaction length, and differential expansion impose considerably higher thresholds. In another series of papers, Forslund, Biskamp, Kruer, and others[5] give similar results and in addition investigated the nonlinear development of SBS and SRS through computer simulation.

Relevant results have been summarized by Chen[6]. In the CO_2 experiments discussed below, the intensity of $\simeq 10^{11}$ W/cm^2 far exceeds the homogeneous thresholds for both SRS and SBS. However, the instability is convective, and the relevant threshold is set by the finite length ℓ of the interaction region--either the plasma length or the depth of focus of the laser light. The instability grows exponentially at the rate γ_o, but the number of e-foldings N above thermal noise is limited by the rate of energy loss of the decay waves by convection or damping. The threshold is set by the value of N required for detectability. It turns out that SRS has a threshold of order c^2/v_e^2 larger than SBS (v_e being the electron thermal speed), amounting to about 10^{13} W/cm^2 for the experiments in question, and is therefore expected to be absent. Brillouin scattering has the threshold

$$N = \frac{2\gamma_o^2 \ell}{c\gamma_i} \gg 1 , \qquad \text{where} \qquad \gamma_o = \frac{1}{2}\,\frac{v_o}{c}\left(\frac{\omega}{\omega_i}\right)^{1/2} \omega_{pi} , \tag{1}$$

γ_i being the ion wave damping rate and $v_o = eE_o/m\omega_o$ the electron quiver velocity in the field E_o of the incident wave. According to numerical computations[5], SBS would dominate over SRS even under laser-fusion conditions because of the tendency of SRS to saturate at low levels. In the absence of critical-layer phenomena and SRS, the only competing parametric processes are filamentation and stimulated sidescatter. The latter has a lower intrinsic growth rate than backscatter and is important only in solid-target experiments where the plasma is more inhomogeneous in the beam direction than perpendicular to it. Filamentation has a growth length longer than is available in the CO_2 experiments.

Eq. (1) is valid when ion Landau damping γ_i, rather than convection, limits the growth of the ion wave. Thus, the time required to set up an ion wave of the proper amplitude is of order $\gamma_i^{-1} \simeq 0.1$ nsec; otherwise, it would be of order $\ell/c_s \simeq 150$ nsec, longer than the $\simeq 50$ nsec pulse lengths used. The simulation experiments, therefore, have sufficient duration to test the validity of (1). The dependence of Eq. (1) on ℓ is particularly important in the light of recent explanations[7] of the observed decrease of back reflection at very large intensities[8]. These explanations involve a steepening of the density profile.

In the experiment of Turechek and Chen[9], the target was a pulsed, high-current arc in 1-15 torr of H_2, He, A, or He + A, a pressure low enough to ensure that the plasma density was every-

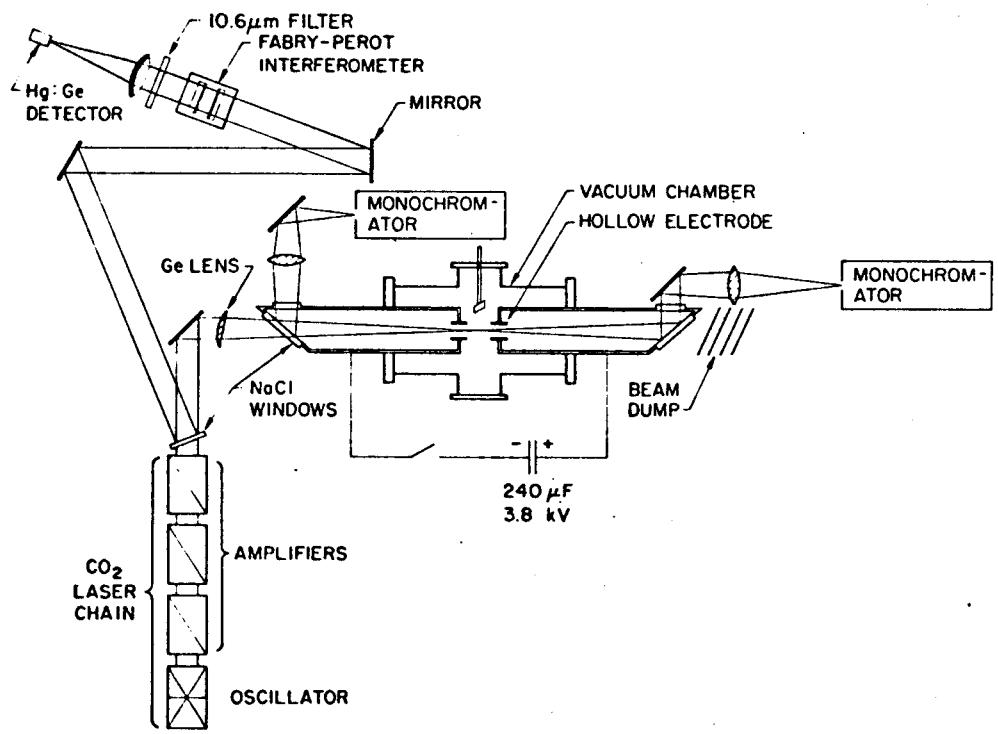

Fig. 1. Diagram of Turechek-Chen experiment.

where below $n_c/4$ for 10.6 μm. Typically, $n \simeq .02\ n_c$ and $n_c/4 = 2.5 \times 10^{18}$ cm^{-3}. The CO_2 laser beam entered and left the plasma axially through tubular electrodes (see Fig. 1). The beam from a 45-J, 0.5-GW double-discharge system was focussed by a 75-cm focal length, f/20 lens to provide a uniformly illuminated region about 1 mm in diameter and 3 cm long, with peak intensity $\simeq 5 \times 10^{10}$ W/cm^2. The plasma was about 2 cm in diameter and 10 cm long, so that its inhomogeneity was weaker than that of the pump field. Backscattered light was extremely weak--about 10^{-7} of the incident intensity, or 9 e-foldings above Thomson scattering. SBS appeared as short, random spikes after the peak of the incident pulse, often occurring well into the tail, when the intensity had fallen to less than 10% of its peak value (see Fig. 2). Multiple-shot spectra of the backscattered light were taken with a low-resolution Fabry-Perot interferometer of large area, as required by the low intensity. These are shown for various gases in Fig. 3.

There are several points of particular interest in this experiment. First, observable backscatter was seen only during a short time interval during the rise of the arc current. At this time, the plasma is only 5% ionized, with $n_e \simeq 1 \times 10^{16}$ cm^{-3} and and $KT_e \simeq 2$ eV. Heating by the initial peak of the laser pulse heats the plasma, completes the ionization, and brings n_e to

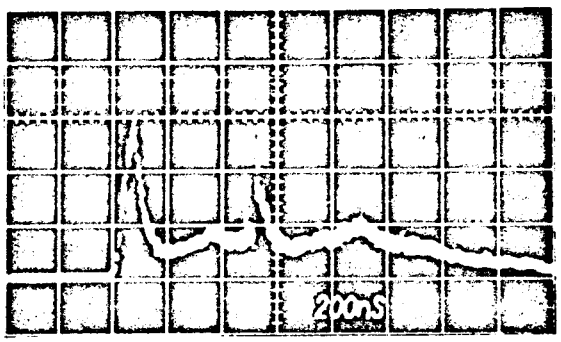

Fig. 2a

Backscattered signal (Initial peak is stray light)

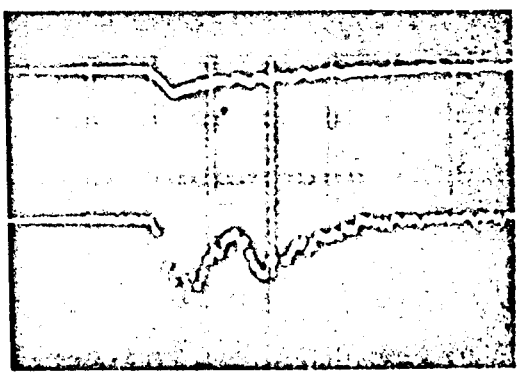

Fig. 2b

upper: Continuum intensity

lower: Intensity of forbidden line

(Turechek and Chen)

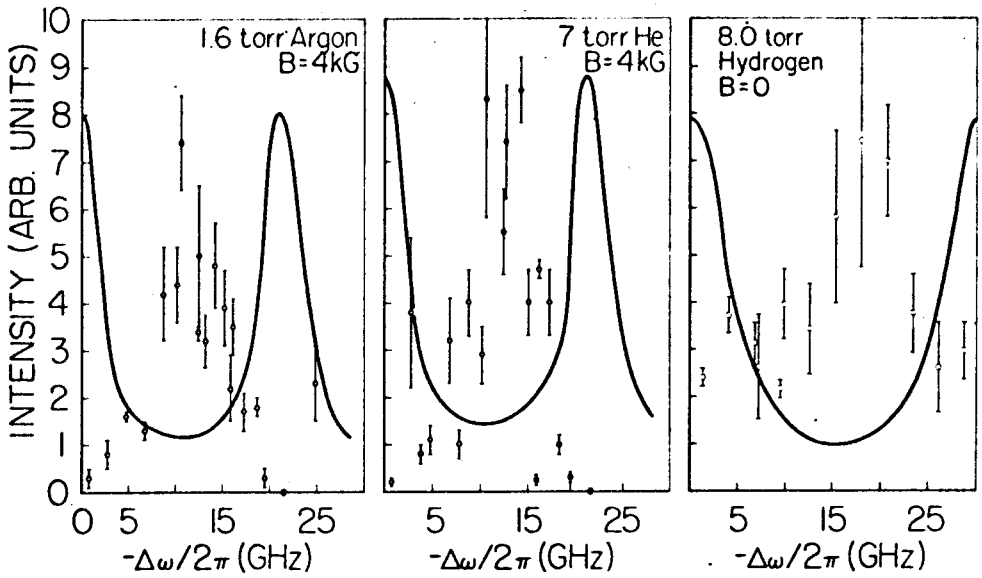

Fig. 3 Spectra of red-shifted backscattered light. (Turechek and Chen)

2×10^{17} cm^{-3} or above. At later times, there is insufficient neutral density for this to happen, and the arc itself cannot raise n_e above 3×10^{16} cm^{-3} because of pressure balance. In spite of the attempt to create a plasma target independently, the experimental conditions are greatly affected by the pump field itself.

Second, the red-shifts f_i shown in Fig. 3 do not scale simply with ion mass. Since the shift $\omega_i = 2\pi f_i$ is equal to $2k_o c_s$ when $\omega_o >> \omega_p$, one would have expected an $M^{-\frac{1}{2}}$ dependence. However, inverse bremsstrahlung absorption varies as Z, so that T_e varies from gas to gas. The measured shifts show that $c_s \simeq (ZKT_e/M)^{\frac{1}{2}}$ remains approximately constant. To verify the change of Z and T_e with M, exhaustive spectroscopic measurements were made of the laser-heated focal region. A lower limit to T_e was determined from line ratios using a time-dependent coronal model. The value of Z was 1, 2, and 8 for H, He, and A, respectively. Densities were measured by line broadening, mostly of He II 4686 A, introduced, if necessary, as a diagnostic impurity. In addition, numerical computations were made for the evolution of n_e and T_e, taking into account ionization and recombination, absorption by electron-ion and electron-neutral collisions, multiple ion charge species, nonlinear radial heat conduction, and electron-ion temperature relaxation. Results for T_e in various gases are shown on Fig. 4, which verifies that ω_i varies properly with ion mass when the difference in T_e is taken into account.

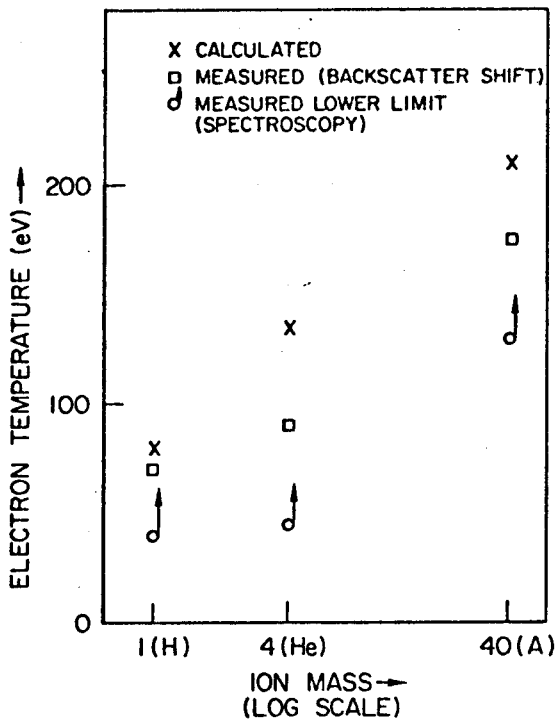

Fig. 4 Computed and measured electron temperatures, as compared with those from SBS red-shift. (Turechek and Chen)

The magnitude of the threshold, Eq. (1), was also verified. From the backscatter intensity, the number N of e-foldings above thermal noise was determined to be about 10. Plotting the required incident intensity I_o as a function of n_e and T_e for ℓ = 10 cm, one finds that the initial laser spike is below threshold in the arc-generated plasma. After n_e and T_e are raised by laser heating, ion Landau damping is reduced so that even the intensity in the tail of the pulse is above threshold, as observed.

Finally, a third point of this experiment is that the low-frequency fluctuations in SBS were detected directly by using the time-dependent Stark effect in helium. The line 6671 A of He I is accompanied by a forbidden line at 6632 A. The forbidden transition can be induced by a large electric field. This is seen in synchronism with backscatter. In Fig. 2b, the continuum and forbidden-line intensities are shown. It is seen that the continuum has an increase associated with laser heating by the initial spike; the 6632 A line shows this also, but in addition has peaks correlated with the occurrence of SBS. It turns out that the ion-wave field is too weak to cause the forbidden line increase, but the beat-wave field at ω_i between the incident and reflected light is of the right order of magnitude. Apparently, the nonlinearity generating the low-frequency field stems from the quantum mechanical processes in the atom. Although this effect is far from understood, it is an example of the type of diagnostics needed for careful studies of parametric instabilities in laser-plasma interactions.

The second experiment reviewed here is that of Offenberger et al.[10], whose apparatus is shown in Fig. 5. Here again, the idea was to verify the existence of SBS in a plasma known to be underdense everywhere. The plasma was generated by the CO_2 laser pulse itself the technique is well known among those studying laser heating of plasma confined in linear solenoids. The laser light was focussed by a 52-cm focal length lens through a small aperture into a chamber filled, typically, with 18 Torr of H_2. To prevent breakdown between the aperture and the lens, the intervening space was pumped out just before each pulse. Laser breakdown created plasma which expands radially and axially, the density at the time of backscatter being lower than the filling density of 1.2×10^{18} cm^{-3} on axis and higher than this in the shock front. A 110-kG pulsed magnetic field could be used to retard the radial expansion and increase T_e. At the time of backscatter (≈20 nsec after the beginning of the pulse) the plasma conditions were computed to be $T_e \simeq 70$ eV, $T_i \simeq 10$ eV, $n_e \simeq 4 \times 10^{17}$ cm^{-3} (an average of the $B = 0$ and $B \neq 0$ cases). The column length ℓ was measured by streak photography to be 4.4 mm. The double-discharge CO_2 laser produced 125 J in a 40-nsec, 1-GW spike plus a 1-μsec, 200 MW tail. The focussed intensity was 10^{11} W/cm^2.

Reflected light occurred during the peak of the pulse and was sufficiently intense (0.2%) to be analyzed by a monochromator and a high resolution (3.5 A) Fabry-Perot interferometer in series. Fig. 6a shows the SBS spectrum for $B = 0$, taken by averaging shots in a 10-A window, corresponding to 2.7 GHz resolution. Because of the large reflected intensity relative to stray light, the high-finesse interferometer, and better reproducibility because I_o was well above threshold, this spectrum is considerably more accurate than those of Turechek and Chen. Both a red-shift (≈17 GHz) and a width (≈5 GHz FWHM) could be determined. Furthermore, the scattered intensity vs. incident power and initial pressure could be measured, as shown in Figs. 6b and 6c. The latter is purported to represent variation with interaction length ℓ.

From the slope of Fig. 6b, the known value of ℓ, and the computed values of T_e, and T_i, and n, one can calculate the value of γ_o to be 10^{11} sec^{-1}. From the second of Eqs. (1), one obtains $\gamma_o \simeq 5 \times 10^{10}$ sec^{-1}, which is excellent agreement. However, the authors prefer to use the random-phase theory of Tsytovich, which predicts a growth rate γ_k of 5×10^{11} sec^{-1}, as compared with 6×10^{11} sec^{-1} from Fig. 6b. This agreement is surely fortuitous, and the method itself is suspect because random-phase theory predicted a faster growth than coherent-phase theory.

Offenberger et al. also compared the width of the spectrum with that due to ion Landau damping and found that it was larger than expected. Inclusion of collisional damping, however, is not

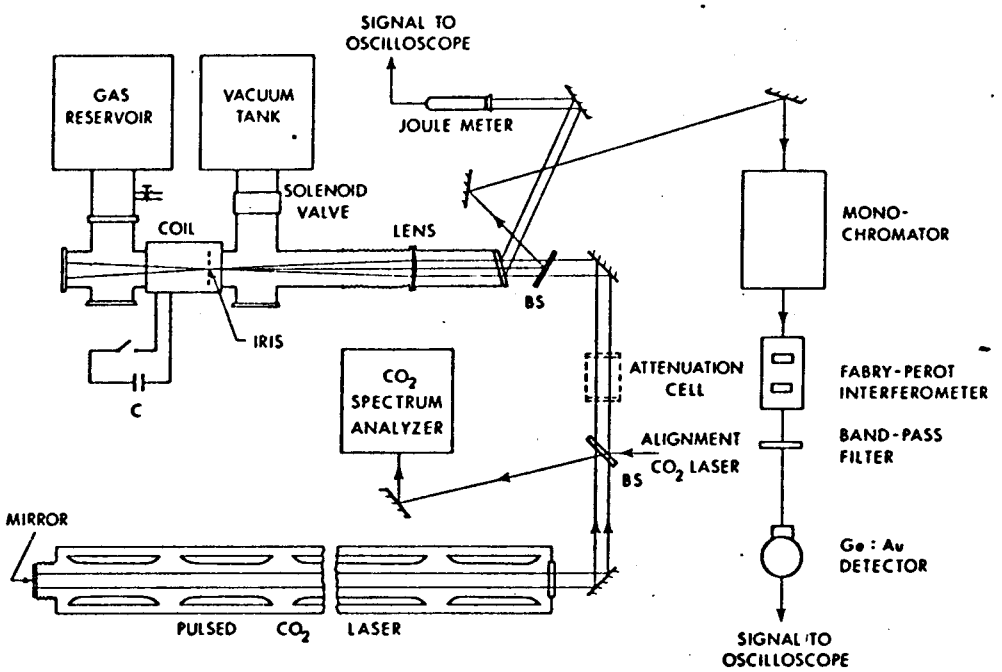

Fig. 5 Diagram of experiment of Offenberger et al.

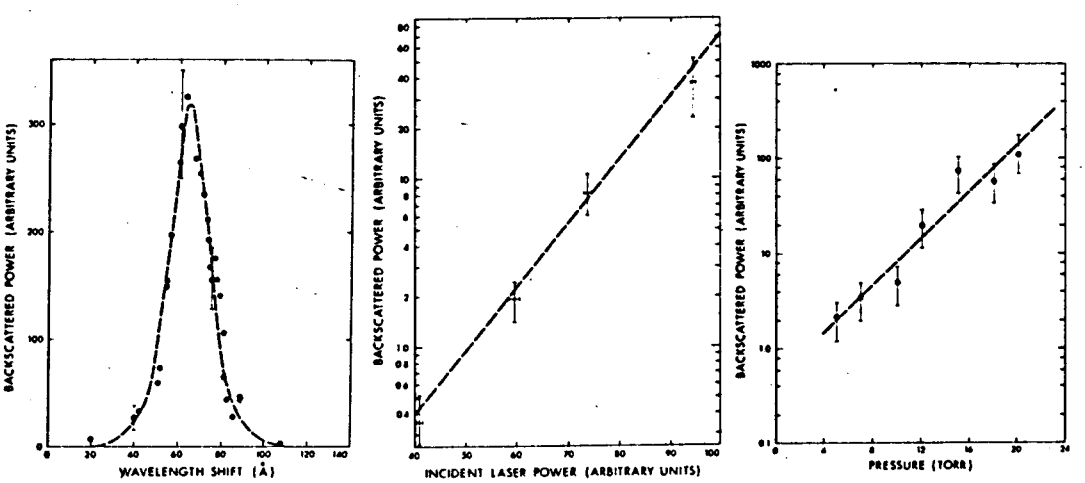

(a) (b) (c)

Fig. 6 Data of Offenberger, Cervenan, Yam, and Pasternak.
(a) SBS spectrum, (b) Power dependence, (c) Pressure dependence

straightforward, since the latter can decrease the total damping by disturbing the resonant particles. Furthermore, the width also depends on the number of exponentiations and the duration of the spiky signals. In checking the mass dependence between H and He, the authors failed to account for the difference in T_e. They also pointed out that the product of I_o and ℓ was larger in the tail of the pulse than at the peak, but no SBS was observed there. Finally, computing N from γ_o and Eq.1, one finds N = 8.7, about the same as in the Turechek-Chen experiment. Since I_s/I_o was $\simeq 10^{-6}$ in that case for 9 e-foldings above thermal noise, the value of $I_s/I_o = 2 \times 10^{-3}$ in Offenberger's experiment suggests an initial level of ion acoustic turbulence far above thermal. In summary, this experiment has by far the best data obtained so far, but there are many questions still left unanswered and many diagnostic checks to be made.

The third experiment along this line is that of Massey, Berggren and Pietrzyk.[11] Again, laser breakdown was used to produce the plasma in a large (100-kG) magnetic field (Fig. 7). The plasma density was measured as a function of distance along B by ruby interferometry (Fig. 8). For a typical pressure of 28 Torr of H_2, the maximum density is 1.8×10^{18} cm^{-3}; however, much of the data was taken at higher pressures, where $n > n_c/4$. The e-beam sustained CO_2 laser produced 125 J in a 2-μs pulse, with 150 MW in the tail and about twice as much at the peak. The intensity during

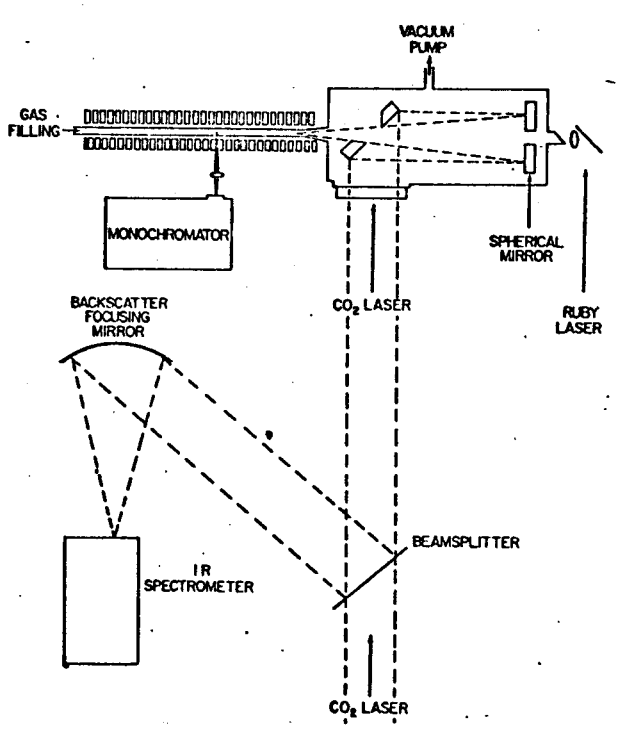

Fig. 7 Diagram of experiment of Massey, Pietrzyk, and Scudder.

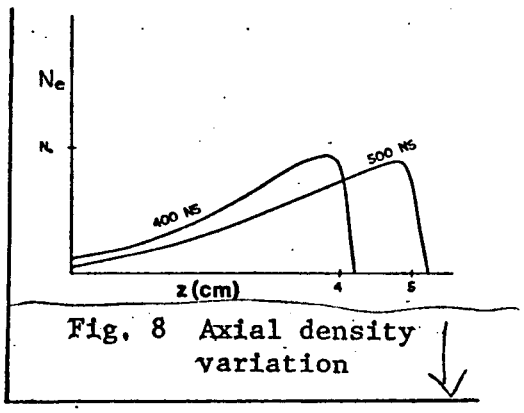

Fig. 8 Axial density variation

backscatter was about 5×10^9 W/cm^3. In spite of the lower intensity, higher backscatter (1 - 5%) was observed than in Offenberger's experiment. The beam was focussed by an 0.5-m focal length mirror, which resulted in backscatter during the gain-switched peak. Earlier work with a 1-m f.l. mirror produced late backscatter, presumably because the plasma, at low I_o, was too short at early times.

Data on spectrum, I_o dependence, and n_e dependence are shown in Fig. 9. These data were taken with pyroelectric detectors and a grating spectrometer. The scattered power, as large as 9 J, could be measured calorimetrically. Single-shot spectra were obtained with liquid crystal detectors. The electron temperature was measured by C V impurity line emission, using a time-dependent coronal model, yielding $KT_e = 80 \pm 25$ eV.

In interpreting the data, the density profile of Fig. 8 was approximated by a square profile, 1.5 - 2 mm long, at the peak density. From Fig. 9b, extrapolation to zero power would give the initial turbulence level if T_e were constant. If the variation of T_e with power P is taken into account by $T_e \propto P^{2/7}$, the resulting number of exponentiations is N = 4.8, indicating a very high level of initial turbulence. Using this value of N, and the measured

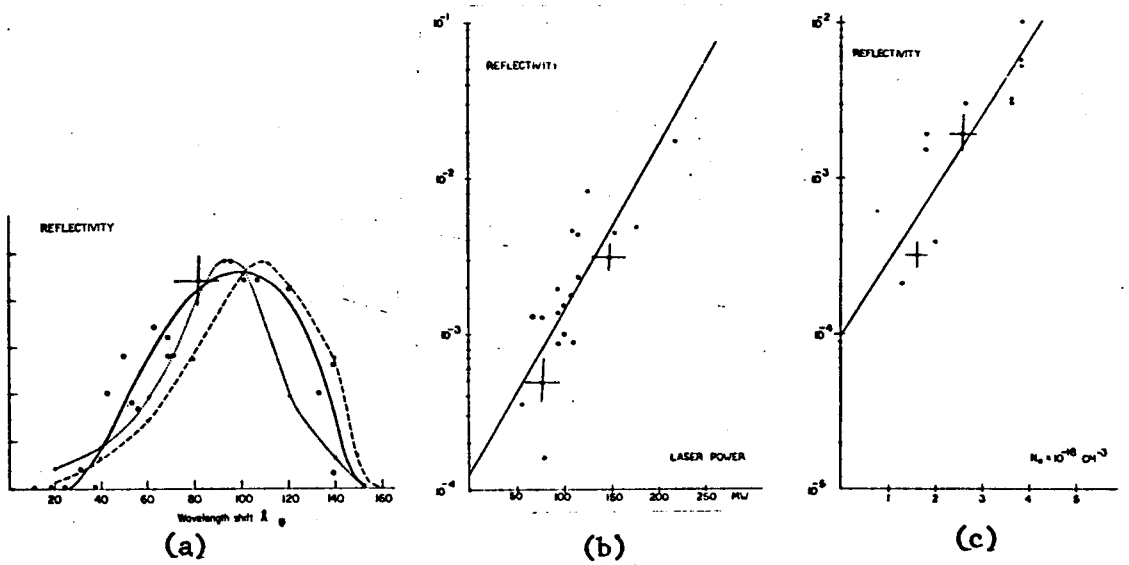

Fig. 9 Data of Massey et al.: Backscattered power vs. (a) red-shift, (b) laser power, and (c) plasma density. The dashed curve in (a) is theory for $T_e = T_i = 80$ eV, and the dotted curve, for 60 eV.

values of T_e and n_e, one can compute the spectrum from theory; good agreement is shown in Fig. 9a. In Fig. 9c, the pressure dependence is interpreted as a dependence on n_e, whereas Offenberger et al. interpret it as a dependence on ℓ. This point is unresolved.

These three backscattering experiments are compared in Table I (hydrogen data only). A, B, and C refer to Refs. 9, 10, and 11, respectively. F. L. is focal length; R the backscattered power divided by the incident power at that time; N the number of e-e-foldings; f_i the ion-acoustic frequency shift (measured); Δf the frequency resolution; and FWHM the measured width of the spectrum.

Each of the experiments had its particular advantages. Experiment A was the only one in which n_e was definitely below $n_c/4$, and in which SBS grew from thermal noise, presumably because the arc current was well below the threshold of the ion acoustic instability. Furthermore, A had the forbidden-line diagnostic. The small signals did not permit varying I_o. In B and C, the initial turbulence level was not understood, but it gave large signals permitting variation of I_o and, in the case of C, a single-shot spectrum. Between these, B had the higher I_o and the better spectral resolution, but C had better diagnostics of the plasma. All three experiments revealed the spiky nature of SBS; which of many reasons is responsible for the fast decay of SBS once it starts is unknown. It is clear that much more work needs to be done, including checking the inhomogeneous

TABLE I

Expt.	ℓ(cm)	KT_e(eV)	$n_e(cm^{-3})$	W(J)	P(GW) (peak)	$I_o(GW/cm^2)$ (peak)	(tail)
A	3	45	2×10^{17}	45	0.5	50	3
B	0.44	70	4×10^{17}	125	1.0	100	20
C	0.2	80	2×10^{18}	125	0.3	10	5

Expt.	F.L.(cm)	R(%)	N	f_i(GHz)	Δf(GHz)	FWHM(GHz)
A	75	10^{-4}	9.2	18	4.3	10
B	52	0.2	8.7	17	2.7	5.3
C	50	1-5	4.8	25	6.7	21

threshold, measuring the initial level of turbulence, confirming the existence of ion waves, and finding the angular distribution of scattering.

Other Experiments on Plasma Targets

A number of other experiments have been reported concerning nonlinear laser-plasma effects in underdense plasmas. Using a dc magnetically stablized arc, Marhic[12] was the first to detect the radial ponderomotive force applied by a laser beam to a plasma well below critical density. The plasma was almost fully ionized, with $n_e = 3 \times 10^{14}$ cm^{-3} and $T_e = 1.4$ eV. The first demonstration of the beat-frequency mixing of two laser beams with $\Delta\omega \approx \omega_p$ was done by Stansfield, Nodwell, and Meyer[13] in a partially ionized atmospheric arc with a density of 2×10^{16} cm^{-3} and $KT_e = 1.5$ eV. Fabre[14] has developed a technique of using a ruby laser to produce a plasma from a polyethylene foil, and then doing a CO_2-laser experiment on the plasma. The plasma target has $n_e \approx 5 \times 10^{18}$ cm^{-3}, $T_e \approx 9$ eV, $r = 1$ mm, $L = 1.5$ cm, and lasts 50-100 nsec. Finally, plasma foci[15] can produce plasmas of density 2×10^{19} cm^{-3}, temperature 7 keV, raidus 1 mm, and length 1 cm, lasting 70 nsec.

COMPARISON OF LASER-PLASMA SOURCE COMBINATIONS

For future experiments on parametric effects, we wish to consider the relative merits of various available radiation and plasma sources.

1. In the microwave range, high powers are easily available in the 3-30 cm wavelength regime; for instance, 100 kW in 20-μsec pulses with a klystron or traveling wave tube is common. Even 1 MW in 3-μs pulses with a magnetron is not an unusually cumbersome apparatus. We shall choose this in a 10-cm wavelength as our reference microwave source. The cutoff density being about 10^{11} cm^{-3}, the ideal plasma target for work in the underdense region up to $n = n_c$ is a low-pressure filament discharge of the type developed at UCLA. These have $KT_e \approx 3$ eV and characteristic dimension $L \approx 100$ cm $\gg \lambda_o$.

2. In the 4-8 mm microwave range, a reasonably high power would be 40 kW in a 1-μsec pulse from a magnetron. At 8 mm, n_e is 2×10^{13} cm^{-3}. Possible plasma targets at these higher densities are pulsed, partially ionized plasmas produced by ultraviolet radiation from sparks or by laser irradiation of solids. However, we shall take as a reference system a rf-generated plasma produced, say, by a Lisitano coil; the temperature would be about 8 eV.

3. Recent development of far-infrared lasers has yielded about 300 W at 337 μm with the HCN laser and 200 kW at 496μm (≈0.5 mm) with the CH_3F (methyl fluoride) laser, optically pumped by a 9.55-μm CO_2 laser. For reference, we shall take a 1-MW CH_3F laser (which will soon be achieved) with a 50-nsec pulse length. To go up to the critical density of 5×10^{15} cm^{-3}, one can use a high current arc, which has $KT_e \approx 5$ eV.

4. Moving to 10.6-μm CO_2 lasers, we find that 1 GW (peak) in a 50-nsec pulse is achievable with relative ease and flexibility with TEA, double-discharge or e-beam sustained lasers. It is not easy to reach the critical density of 10^{19} cm^{-3} except with a plasma focus, but in the underdense regime of $n \simeq 10^{16-18}$ one can use pulsed, high-current arcs, z-pinches, θ-pinches, or laser breakdown plasmas. Whatever the initial temperature, laser heating will raise kT_e to ≃ 100 eV; hence, we shall take this for the reference temperature.

5. At the highest frequencies, we have ruby lasers or dye lasers with $\lambda_o \simeq 0.7$ μm and $n_c \simeq 2 \times 10^{21}$ cm^{-3}. We assume 1 GW in a 30-psec pulse and a plasma focus with $KT_e = 1$ keV.

6. The system that all these are to simulate is a near-term Nd-glass laser irradiating a microballoon. For the reference situation, we take $\lambda_o = 1.06$ μm, P = 1 TW in a 100 psec pulse, $n_c = 10^{21}$ cm^{-3}, and a heated corona with $KT_e \simeq 2$ keV.

These characteristics are summarized in Table II. In addition, we need to compute the incident intensity I_o. The diffraction limited spot size is approximately $f\lambda_o$, where f is the f-number of the focussing optics. The diffraction limit is expected to be reached in microwave and F.I.R. systems, where mode purity is easily controllable. For multi-mode lasers, we assume that the spot diameter exceeds the diffraction limit by a spoilage factor S, which is normally higher for shorter wavelength. Thus, $I_o = P/(\pi/4)(S\lambda_o f)^2$. To obtain the f-number, we assume a typical beam diameter and a focal length compatible with the size of the plasma. The pulse length is τ.

TABLE II

λ_o	P	f	S	$I_o(W/cm^2)$	$n_c(cm^{-3})$	T_e(eV)	τ
10 cm	1 MW	1	2	3×10^3	10^{11}	3	3 μs
8 mm	40 kW	1	2	2×10^4	2×10^{13}	8	1 μs
0.5 mm	1 MW	1	3	6×10^7	5×10^{15}	5	50 ns
10.6 μm	1 GW	15	5	2×10^{11}	10^{19}	100	50 ns
0.7 μm	1 GW	25	50	2×10^{11}	2×10^{21}	1000	30 ps
1.06 μm	1 TW	1.5	20	1×10^{17}	10^{21}	2000	100 ps

These are typical, not maximum, values.

Suitability of these systems for simulating effects in pellet irradiations (last line, Table II) can be evaluated by several criteria.

1. Ponderomotive force. Profile modifications and parmetric instabilities are driven by the force[6].

$$F_{NL} = -\frac{\omega_p^2}{\omega^2} \nabla \frac{\langle E^2 \rangle}{8\pi}$$

The ratio of F_{NL} to the ∇p force is a measure of the importance of parametric effects. Hence, we define a quantity G as

$$G \equiv \frac{F_{NL}}{\nabla p} = -\frac{\omega_p^2}{\omega^2} \frac{\nabla \langle E^2 \rangle / 8\pi}{\nabla p} = -\frac{\omega_p^2}{\omega^2} \frac{\langle E^2 \rangle / 8\pi}{nKT} = \frac{n}{n_c} \frac{4\pi I/c}{8\pi nKT} = \frac{I}{2cn_c KT}$$

where $T = T_e + T_i$ and $n_c = m\omega^2/4\pi e^2$.

2. Exponentiation. The growth rate of instabilities is scaled to the ion plasma frequency Ω_p. The number of exponentiations in the pulse length τ is, therefore, some fraction of $\Omega_p \tau$. In calculating $\Omega_p \tau$, we assume hydrogen and a density of 0.1 n_c.

3. Classical absorption. In an experiment in which the critical density is reached, the amount of beam energy absorbed classically by the plasma depends on the density scale length L. For a linear gradient $\nabla n \simeq n_c/L$ in plane geometry, the energy loss after reflection is

$$\frac{\Delta I}{I_o} = 1 - \exp\left[-\frac{32}{15} (7.8 \times 10^{-9}) \frac{Z \ln\Lambda \, n_c^2 \, L\lambda_o^2}{c^2 T_{ev}^{3/2}} \right]$$

for $Z = 1$ and $\ln \Lambda = 5$, this becomes

$$\frac{\Delta I}{I_o} = 1 - \exp\left(-1.16 \times 10^{-2} L/\lambda_o^2 T_{ev}^{3/2}\right)$$

The effect of ΔI on the plasma is measured by the ratio Q of $\tau\Delta I$ to the plasma energy $\frac{3}{2}\bar{n}KTL$ per cm^2, where $\bar{n} = \frac{1}{2}n_c$.

Thus $$Q \equiv \tau\Delta I/0.75\, n_c KTL \simeq \tau\Delta I/n_c KT_e L,$$

where $T_i = T_e/3$ has been assumed for convenience. In Table III, both $\Delta I/I_o$ and Q are given for a typical value of L.

4. Plasma heating. Even in underdense regions, inverse bremsstrahlung absorption causes pressure-gradient and thermo-electric forces which compete with radiation pressure in driving instabilities, self-focussing, and spontaneous magnetic fields. The rate of absorption is

$$q = \frac{3.1 \times 10^{-7} Z n_e^2 \ln\Lambda\, I}{T_{ev}^{3/2}\omega^2(1 - \omega_p^2/\omega^2)^{1/2}} \text{ ergs/cm}^3\text{/sec}$$

If thermal conduction is neglected, the change in temperature is given by

$$\frac{d}{dt}\left(\frac{3}{2} nKT\right) = q(T)$$

Integrating over time and assuming Z = 1, $\ell n\, \Lambda = 5$, and $n/n_c = 0.1$, we find

$$T_{ev}^{5/2} - T_o^{5/2} = 1.7 \times 10^{13}\, nI\tau/\omega^2 = 4.8 \times 10^{-11}\, \lambda_o^2 n_c I\tau$$

where I is in $W/cm^2/sec$. The value of $\Delta T/T$ is shown in Table IV.

The relative effect of heating is measured by the ratio H of $\Delta(nKT)$ to the pondermotive potential $(\omega_p^2/\omega^2)\langle E^2\rangle/8\pi$. H is given by

$$H \simeq 10^{-8}\, \frac{n_c T_{ev}}{I_o} \frac{\Delta T}{T}$$

and is given in Table IV for $n = 0.1\, n_c$.

On the other hand, thermal conduction can limit the temperature rise. The latter then depends on the beam power rather than its intensity. We have considered radial conduction from a long, thin, heated cylinder of radius a, with the temperature at radius $b >> a$ held constant at the initial temperature T_o. If there is no magnetic field, the approximate steady-state solution for the temperature T_{ev} of the heated region is

$$T_{ev}^{3/2}\,(T_{ev}^{7/2} - T_o^{7/2}) = 1.9 \times 10^{-30}\, \lambda_o^2 n^2\, P\, \ell n\, (b/a).$$

TABLE III

λ_o	G	$\Omega_p\tau$	L(cm)	$\Delta I/I_o$	Q
10 cm	0.9	400	100	.002	0.18
8 mm	.02	1700	2	.002	0.72
0.5 mm	0.28	1400	1	0.34	280
10.6 μm	.02	7×10^4	0.3	.96†	200†
0.7 μm	5×10^{-6}	600	0.5	.98†	4×10^{-4}†
1.06 μm	5.2	1300	20(μm)	0.02	360

TABLE IV

λ_o	$\Delta T_e/T_e$ (heat capacity)	H	$\Delta T_e/T_e$ (heat conduction)	H	A
10 cm	0.10	0.10	5×10^{-5}	5×10^{-5}	15
8 mm	.003	2.1	4×10^{-6}	3×10^{-4}	9.5
0.5 mm	3.1	12.7	0.16	0.67	19
10.6 μm	4.0	200	0.11	5.5	46†
0.7 μm	4×10^{-5}†	3.6†	2×10^{-4}†	25†	135†
1.06 μm	3.0	0.6	.004	8×10^{-4}	18.6

†These values pertain to plasma densities not attainable with the quoted sources.

Here, P is the beam power in watts, and we have taken $Z = 1$, $n = 0.1\, n_c$, and reasonable $\ell n\, \Lambda$ factors. $\Delta T/T$ and H are also given in Table IV for conduction-limited temperature rise, with $b/a = 10$.

5. Other effects. Finally, we consider swelling and refraction. The intensity of the light-wave field increases near the cutoff layer because of the decrease in group velocity and the constructive interference with the reflected wave. For perpendicular incidence, this amplification factor is given by[16].

$$\left(\frac{E_{max}}{E_o}\right)^2 = 3.74\ (k_o L)^{1/3} \simeq 7\ (L/\lambda_o)^{1/3} \equiv A$$

This quantity is also shown on Table IV. We have assumed a scale length L appropriate to radial incidence. The amplification can, of course, be increased with axial incidence on a long, thin plasma; but in practice collisional absorption limits this. Refraction has been estimated by considering the geometrical-optics deflection of a ray incident on a spherical plasma of radius a with parabolic

density profile and maximum density n. The worst case has impact parameter $p = 3^{-\frac{1}{2}} a$ and deflection $\Delta r \simeq 0.2\ a\ (n/n_c)$. Therefore, refraction can affect the alignment of optics if a is large compared to the spot size and if n/n_c is not very small. Two other effects, the damping of waves and the generation of magnetic fields, cannot easily be compared among experimental systems. An idea of collisional damping (except for neutral collisions) can be obtained from the heating results, but Landau damping depends critically on T_e/T_i. Magnetic fields can arise from many effects, including heating and ponderomotive force, but the effect is strongly geometry-dependent.

Tables II - IV show that different wavelength ranges have different advantages. All the systems have sufficiently large G and $\Omega_p\tau$ to generate parametric instabilities. Only the 10-cm and FIR systems have enough power to approach the nonlinear regime of laser-fusion. Microwave experiments are excellent for isolating parametric phenomena from heating, since Q and H are small. Moreover, the long-wavelength experiments in large, tenuous plasmas offer the possibility of detailed probing of the plasma. On the other hand, only the laser simulations can reproduce the large heating effects that occur in laser fusion, such as anomalous conduction, thermal self-focussing, and thermoelectric generation of magnetic fields. Daignostics of CO_2 and FIR experiments, though easier than for pellet experiments is still a considerable problem.

The results of Tables II to IV can, of course, be adjusted by changing, say, the initial T_e, or τ, or L, or n/n_c. The lower of the values of $\Delta T/T$ in the tables should be taken, except for the Nd-glass case, where the boundary conditions do not resemble those used in the calculation. Although there is some freedom in designing an experiment, it is clear that one cannot always scale every parameter properly or completely isolate a given phenomenon. Nonetheless, well diagnosed and analyzed experiments under less extreme conditions than those in a pellet implosion can provide the missing link between theory (including computation) and reality.

FUTURE EXPERIMENTS

In the remaining space we can only mention a few of the important problems that need scrutiny. Backscattering and sidescattering are by no means well documented. Resonant absorption has never been observed directly; it is not known whether the absorption occurs by collisions or by an instability such as the radiative decay instability. The two-plasmon decay and other parametric processes at the $n_c/4$ layer need to be studied. Filamentation in a plasma has not been detected directly. The mechanism of anomalous heat conduction--perhaps a thermal instability involving spontaneous magnetic fields--needs to be determined. And, of course, it would be nice to know how laser-plasma interactions produce such efficient fast-ion accelerators.

ACKNOWLEDGMENTS

We are indebted to R. Massey and J. Turechek for access to unpublished data. This work was supported by the U.S. Energy Research and Development Administration, Contract E(04-3)-34, P.A. 236.

References

1. H. C. Kim, R. Stenzel, and A. Y. Wong, Phys. Rev. Letters 33, 886 (1974).
2. S. P. Obenschain, N. C. Luhmann, Jr., and P. T. Greiling, Phys. Rev. Letters 36, 1309 (1976).
3. J. F. Drake, P. K. Kaw, Y. C. Lee, G. Schmidt, C. S. Liu, and M. N. Rosenbluth, Phys. Fluids 17, 778 (1974).
4. M. N. Rosenbluth, Phys. Rev. Letters 29, 565 (1972); M. N. M. N. Rosenbluth and R. Z. Sagdeev, Comments on Plasma Physics and Controlled Fusion 1, 129 (1972); C. S. Liu, M. N. Rosenbluth, and R. B. White, Phys. Rev. Letters 31, 697 (1973) and Phys. Fluids 17, 1211 (1974); M. N. Rosenbluth, R. B. White, and C. S. Liu, Phys. Rev. Letters 31, 1190 (1973); D. Pesme, G. Laval, and R. Pellat, Phys. Rev. Letters 31, 203 (1973); R. W. Harvey and G. Schmidt, Phys. Fluids 18, 1395 (1975).
5. D. W. Forslund, J. M. Kindel, and E. L. Lindman, Phys. Rev. Letters 30, 739 (1973), Phys. Fluids 18, 1002 (1975) and 18, 1017 (1975); D. F. DuBois, D. W. Forslund, and E. A. Williams, Phys. Rev. Letters 33, 1013 (1974); D. Biskamp and H. Welter, Phys. Rev. Letters 34, 312 (1975); W. L. Kruer, K. G. Estabrook, and K. H. Sinz, Nuclear Fusion 13, 779 (1973).
6. F. F. Chen, Laser Interaction and Related Plasma Phenomena, ed. by H. J. Schwarz and H. Hora (Plenum Press, New York, 1973), vol. 3A, 291.
7. W. L. Kruer, E. J. Valeo, and K. G. Estabrook, Phys. Rev. Letters 35, 1076 (1975).
8. M. Lubin, E. Goldman, J. Soures, L. Goldman, W. Friedman, S. Letzring, J. Albritton, P. Koch, and B. Yaakobi, Plasma Physics and Controlled Nuclear Fusion Research 1974 (Int'l Atomic Energy Agency, Vienna, 1975) II, 459; C. Yamanaka, T. Yamanaka, T. Sasaki, J. Mizui, and H. B. Kang, Phys. Rev. Letters 32, 1038 (1974); J. Martineau, S. Repoux, M. RAbeau, G. Nierat, and M. Rostaing, Opt. Commun. 12, 307 (1974); K. Dick and H. Pepin, Opt. Commun. 13, 289 (1975).
9. J. J. Turechek and F. F. Chen, Phys. Rev. Letters 36, 720 (1976).
10. A. A. Offenberger, M. R. Cervenan, A. M. Yam, and A. W. Pasternak, Jour. Appl. Phys. 47, 1451 (1976).
11. R. Massey, K. Berggren, and Z. A. Pietrzyk, Phys. Rev. Letters 36, 963 (1976). The data given here are from more recent work: R. Massey, Z. A. Pietrzyk, and D. W. Scudder, Sixth Annual

Anomalous Absorption Conference, May 10-21, 1976, Vancouver, B.C., Canada, Abstract 57.
12. M. E. Marhic, Phys. Fluids 18, 837 (1975).
13. B. L. Stansfield, R. Nodwell, and J. Meyer, Phys. Rev. Letters 26, 1219 (1971).
14. E. Fabre and C. Stenz, Phys. Rev. Letters 32, 323 (1974).
15. Y. Kitagawa, A. Thein, E. Setoyama, C. Yamabe, and M. Yokoyama, J. Phys. Soc. Japan (to be published); J. W. Mather, Methods of Experimental Physics 9B, ed. by H. R. Griem and R. H. Lovberg, Academic Press, New York & London (1971).
16. R. W. White and F. F. Chen, Plasma Phys. 16, 565 (1974).